Recent Status and Improvement of Reduced-Activation Ferritic-Martensitic Steels for High-Temperature Service [†]

L. Tan,[1*] Y. Katoh,[1] A.-A.F. Tavassoli,[2] J. Henry,[2] M. Rieth,[3] H. Sakasegawa,[4,1] H. Tanigawa,[4] Q. Huang[5]
[1] Oak Ridge National Laboratory, Oak Ridge, TN 37831, USA
[2] DMN/Dir, DEN, CEA Saclay, 91191 Gif-sur-Yvette cedex, France
[3] Karlsruhe Institute of Technology, Karlsruhe 76021, Germany
[4] National Institutes for Quantum and Radiological Science and Technology, Rokkasho, Aomori 039-3212, Japan
[5] Institute of Nuclear Energy Safety Technology, Chinese Academy of Sciences, Hefei, Anhui 230031, China
[*]Corresponding author: One Bethel Valley Road, P.O. Box 2008, MS-6136, Oak Ridge, TN 37831; Phone: +1 865 574 4628; E-mail: tanl@ornl.gov (L. Tan)

Abstract

Reduced-activation ferritic-martensitic (RAFM) steels, candidate structural materials for fusion reactors, have achieved technological maturity after about three decades of research and development. The recent status of a few developmental aspects of current RAFM steels, such as aging resistance, plate thickness effects, fracture toughness, and fatigue, is updated in this paper, together with ongoing efforts to develop next-generation RAFM steels for superior high-temperature performance. In addition to thermomechanical treatments, including nonstandard heat treatment, alloy chemistry refinements and modifications have demonstrated some improvements in high-temperature performance. Castable nanostructured alloys (CNAs) were developed by significantly increasing the amount of nanoscale MX (M=V/Ta/Ti, X=C/N) precipitates and reducing coarse $M_{23}C_6$ (M=Cr). Preliminary results showed promising improvement in creep resistance and Charpy impact toughness. Limited low-dose neutron irradiation results for one of the CNAs and China low activation martensitic are presented and compared with data for F82H and Eurofer97 irradiated up to ~70 displacements per atom at ~300–325°C.

1. Introduction

Reduced-activation ferritic-martensitic (RAFM) steels have been developed as candidate structural materials for blanket components of fusion reactors. The development of RAFM steels has benefitted greatly from the developmental knowledge base for conventional FM steels such as T91 and their radiation resistance in fission reactors. The techniques for fabrication and joining of RAFM steels are similar to those used for conventional FM steels, leading to quick

technological maturation compared with other advanced low-activation materials such as vanadium alloys and SiC_f/SiC composites.

RAFM steels were primarily developed with 8–9 weight percentage (wt %) chromium (Cr) because steels with that Cr content exhibited the minimum shift in radiation-induced ductile-brittle transition temperature (DBTT) among a set of 1 to 12 wt % Cr FM steels irradiated at 365 and 410°C for up to 36 displacements per atom (dpa) [1]. To reduce radioactive activity, especially the production of long-lived isotopes, some alloying elements in conventional FM steels, including Mo and Nb, are replaced by W and Ta in RAFM steels. In addition to the impurity limits for conventional FM steels to prevent property impairment—e.g., the effects of P, S, and Si on toughness [2]—there are strict limitations on impurity levels in RAFM steels (e.g., Ni, Co, Cu, Nb, Mo, Ag) to meet the criterion of low activation for shallow land burial of nuclear waste [3,4,5]. Therefore, more careful control of smelting and remelting processes is required for industrial production of RAFM steels.

Since the introduction of nominal 9Cr–2WVTa steel by Oak Ridge National Laboratory (ORNL) in the 1980s [6,7,8], the United States has focused on basic research to systematically study property changes under diverse conditions of irradiation and coolant compatibility. The recent focus has been on the enhancement of high-temperature performance by means of alloy chemistry optimization and thermomechanical treatments [9,10,11]. F82H (8Cr–2WVTa) and JLF-1 (9Cr–2WVTa) were introduced afterward as the major RAFM candidates from Japan [12,13]. F82H has received greater attention; the interest in it is attributed to the international collaborations that yielded the International Energy Agency (IEA) heats for collaborative study among the ITER partners, the Broader Approach (BA) heats in BA activities between the European Union (EU) and Japan under the International Fusion Energy Research Centre project, and continuous research on minor/impurity element control for the F82H-mod heats. Based on the precursor work on MANET and OPTIFER in several member countries of the EU, a higher-Cr and lower-tungsten composition grade, called Eurofer97 (9Cr–1WVTa), was adopted by the EU in 1997 for its improved corrosion resistance and neutron efficiency [14]. Thereafter, the development of other variant RAFM steels—such as CLAM (China low activation martensitic) of China [15,16], INRAFM of India [17], and ARAA (advanced reduced-activation alloy) of Korea [18]—was initiated, with compositions referring to Eurofer97. The typical compositions of these representative RAFM steels are listed in Table 1, showing the major distinctions in the Cr, W, Ta, and N contents. The Ta and N content was moderately increased in the later RAFM steels, such as Eurofer97-2 heat 993402 and CLAM heat 1105, to increase strength; the increase slightly compromised the low activation levels because of the transmutation of nitrogen into long-lived ^{14}C [3,4]. Castable nanostructured alloys (CNAs) being developed at ORNL exhibit some promising results, which are presented in Section 3 of this paper.

Table 1. Typical compositions (wt %) with balance of iron of representative RAFM steel heats compared with T91

Element \ Heat	T91 MGC [19]	9Cr–2WVTa 3791 [6]	F82H BA07 [20]	Eurofer97-2 993402 [21]	CLAM 1105 [16]
C	0.09	0.11	0.09	0.11	0.10
Cr	8.70	8.90	8.00	8.95	8.76
Mn	0.35	0.44	0.46	0.55	0.42
Mo	0.90	0.01	<0.01	0.005	NA

N	0.044	0.021	0.017	0.038	0.04
Nb	0.072	<0.01	<0.005	0.004	NA
Ni	0.28	<0.01	<0.01	0.03	NA
Si	0.29	0.21	0.17	NA	0.05
Ta	NA	0.06	0.04	0.14	0.16
V	0.22	0.23	0.19	0.20	0.22
W	NA*	2.01	1.88	1.04	1.40
Other					

*NA: not available/not reported because of the low level.

Following industrial-scale production of F82H and Eurofer97 at more than 10 to 20 tons per heat, CLAM steel has recently gone through a similar scale-up to industrial production practices with a heat of ~6.4 tons. Eurofer97 design allowables passed from the probationary status, reported at the ICFRM-16 conference [22], to a definitive status in RCC-MRx edition 2015 that validates the full material properties recommendations. However, the addition of an irradiated properties section to the RCC-MRx was postponed until the next edition. This is to allow the harmonization of recommendations made for irradiated conventional 9Cr-1Mo steel (e.g., T91) used in fission reactors with those for Eurofer97 to be used in fusion reactors. Material qualification activities for F82H and CLAM for the ITER test blanket module application are in progress; these activities include rigorous property data compilation with fully traceable origins and experimental/testing history.

The developmental progress of RAFM steels had been routinely reviewed [15,22,23]. Some specific topics such as the weldability [24,25] and coolant compatibility [26,27] of RAFM steels have been reviewed elsewhere. Studies of complex interactive or synergistic mechanical properties, and of the effects of environment (irradiation and/or coolant) on the strength/toughness/fatigue/creep/creep-fatigue of the base metal and weldments of RAFM steels [28,29,30,31], are relatively limited owing to the complexity and capability of experimental controls. This paper updates recent achievements in research and development on current and next-generation RAFM steels. It reports recent findings in long-term thermal aging, plate thickness effects, fracture toughness, fatigue, creep, and radiation hardening. More emphasis is placed on recent improvements for high-temperature performance, exemplified with nonstandard heat treatments and new alloy chemistry.

2. Characteristics of current RAFM steels

2.1 Aging effects

As is the case for conventional FM steels, long-term service at elevated temperatures also degrades the mechanical properties of RAFM steels. Among the extensive thermal aging experiments conducted on RAFM steels, one of the distinct achievements is the 100,000 h aging of an F82H IEA heat at 400 to 650°C [32]. Effects of aging time and temperature on the formation of non-preexisting phases, such as Laves phase and M_6C, were reported, as well as the noticeable coarsening of preexisting $M_{23}C_6$ (M = Cr-rich) precipitates and relatively stable nanoparticles of preexisting MX (M = V/Ta, X = C/N) [32,33]. Reductions in both strength and area became significant after aging at higher temperatures above 500°C. In addition, Charpy

impact toughness was significantly impaired, with increased DBTT and reduced upper-shelf energy (USE), by aging at temperatures ≥500°C. The aging studies indicate that F82H can be used for up to 30,000 h at 550°C. Recent aging studies on Eurofer97 and CLAM steels for up to 5,000 h showed a similar tendency [16, 34]. The property degradation may be primarily attributable to aging-related microstructural evolution, such as recrystallization of subgrains, leading to increased mean subgrain size, annihilation of dislocations, and coarsening of $M_{23}C_6$.

2.2 Effects of plate thickness

A range of plate thicknesses, e.g., 1–52 mm, will be required depending on the test blanket module design; therefore, possible variations in mechanical properties with plate thickness must be considered. Figure 1 shows the tensile test results for yield strength (YS), tensile strength (TS), and total elongation (TE), as well as Charpy V-notch impact absorbed energy (AE) for F82H (BA12 heat) and CLAM (~6.4-ton heat) steels tested at room temperature. The samples were extracted from the half-thicknesses of the heats, with a tensile specimen length parallel to the longitudinal/rolling direction and Charpy specimens in the transverse–longitudinal (T–L) orientation. In general, the CLAM heat results fall approximately within the range of the F82H-BA12 heat values [35]. The increase in plate thickness from ~15 to 100 mm resulted in a noticeable reduction (~70 J) in Charpy impact AE, together with small reductions (~50 MPa) in YS and TS accompanied by a negligible increase in TE. The plate thickness dependency, which was also observed in general ferritic steels, suggests that different microstructures developed in the thin/thick plates; e.g., the structure of the thicker plate was coarser, with larger prior austenite grains, despite the same normalization and tempering final heat treatments.

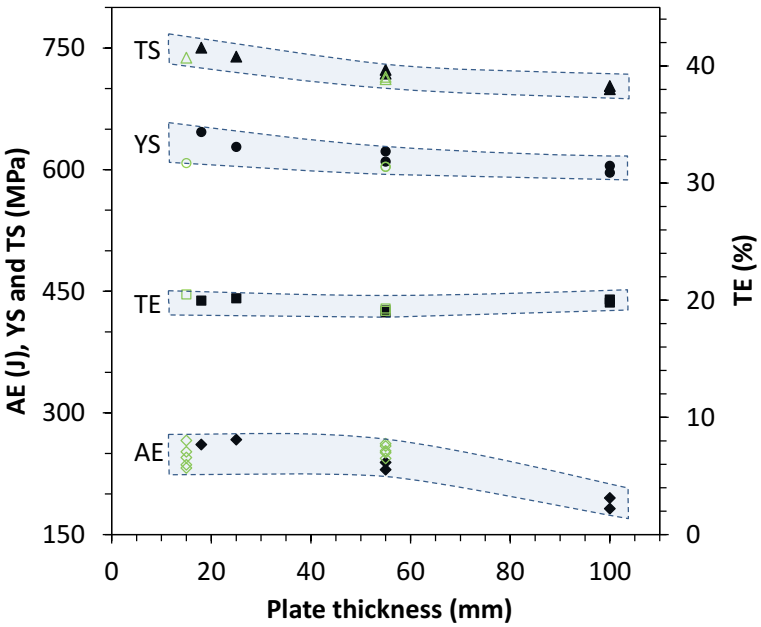

Fig. 1. Effect of plate thickness on YS, TS, TE, and Charpy impact AE at room temperature for F82H-BA12 (filled symbols) and CLAM (open symbols).

2.3 Fracture toughness of Eurofer97

Fracture toughness is an important mechanical property of Eurofer97 examined in RCC-MRx edition 2015. A significant number of new fracture toughness results have been added to the code case in the past couple of years, resulting in an adjustment to the recommendations made earlier. The fracture toughness results for the base metal of the Eurofer97-1 heat in the unirradiated condition are shown in Fig. 2, along with the ASTM E1921-recommended master curve for ferritic/bainitic steels. The lower (5%) and upper (95%) bound curves of the master curve do not adequately cover the scatter of the CIEMAT (Center for Energy, Environment and Technology), natural gamma radiation (NGR), and EPFL (École polytechnique fédérale de Lausanne) data. The large scatter is attributed to the size variations of the compact tension (CT) specimens, ranging from 0.2 to 0.87 T; the specimen orientation (L–T and T–L); and the plate thickness (8 to 25 mm), in addition to the intrinsic local variations of the tempered martensitic microstructures. The NRG data at –134 and –128°C suggest a lower K_{JC} as the plate thickness increases from 8 to 14 mm, which is consistent with Fig. 1 with regard to the trend of lower impact toughness for thicker plates. The EPFL data at –120°C indicate a lower K_{JC} of the L–T compared with the T–L specimens, contrary to the generally observed specimen orientation-dependent Charpy impact toughness. The data in Fig. 2 do not convey a simple dependence of specimen size on fracture toughness. The EPFL data show noticeably lower K_{JC} for the 0.87T specimens than for the 0.35T specimens at –80 and –60°C. In contrast, the NRG data show a somewhat higher K_{JC} for the 0.4 T specimens than for the 0.2 T specimens from a 14-mm-thick plate at –117 and –111°C, but comparable K_{JC} for the 0.4 and 0.2 T specimens from both 14- and 25-mm thick plates at –134 and –95°C, respectively.

For better coverage of the lower/upper bound curves, an alternative master curve of $K_{JC}(1T) = 12 + 88exp[0.019(T - T_0)]$ with the same T_0 = –90°C was proposed, as shown by the dash-dot curve in Fig. 2. In comparison, lower reference temperatures were characterized for F82H, using the master curve method, as –119°C from the IEA and –109°C from the BA07 heats [36,37]. These studies indicate that the master curve method is applicable to assessing the fracture toughness of RAFM steels in the transition temperature region if appropriate adjustments are made to accommodate the small fractions of data beyond the lower and upper bounds, as observed in the F82H and Eurofer97-1 data.

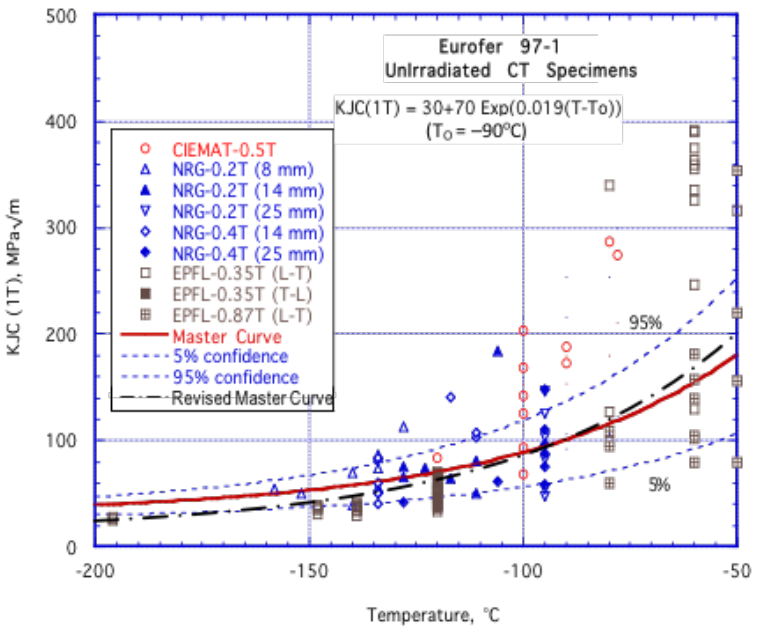

Fig. 2. Master curve plot of the CIEMAT data, together with the NRG and EPFL data, for the base metal of the Eurofer97-1 heat. The numbers in parentheses following the NRG data are the thicknesses of the plates used for the tests.

2.4 Fatigue

Fatigue resistance is likely to be a critical property of RAFM steels used as first-wall blanket structures that are subjected to cyclic loading caused by pulsed-mode plasma operation. Furthermore, cyclic strain usually results in cyclic softening failure of FM and RAFM steels at elevated temperatures, leading to degradation of fatigue resistance. Therefore, low-cycle fatigue tests were conducted on RAFM steels. Figure 3 summarizes the relationship between total strain ($\Delta\varepsilon_t$) and number of cycles to failure (N_f) for CLAM [38,39], Eurofer97 [40], and F82H [41,42] tested at room temperature and 550°C. The $\Delta\varepsilon_t$–N_f relationship is often characterized by the superposition of the plastic strain component ($\Delta\varepsilon_p$) governed by the Manson–Coffin relationship at low-cycle fatigue and the elastic strain component ($\Delta\varepsilon_e$) governed by the Basquin relationship at high-cycle fatigue as [43]

$$\frac{\Delta\varepsilon_t}{2} = \frac{\Delta\varepsilon_p}{2} + \frac{\Delta\varepsilon_e}{2} = \varepsilon_f'(2N_f)^c + \frac{\sigma_f'}{E}(2N_f)^b,$$

where ε_f', σ_f', E, c, and b are the ductility coefficient in fatigue, strength coefficient in fatigue, Young's modulus, Manson–Coffin exponent, and Basquin exponent, respectively. Figure 3 indicates an increase in N_f with decreasing $\Delta\varepsilon_t$ for all of the RAFM steels; but only F82H data show a transition at a threshold N_f, on the order of 10^4 cycles, from the Manson–Coffin relationship at low-cycle fatigue to the Basquin relationship at high-cycle fatigue. The other datasets are within the high $\Delta\varepsilon_t$ range, exerting a discrete amount of plastic deformation in each cycle, described by the Manson–Coffin relationship at low-cycle fatigue.

CLAM, Eurofer97, and F82H generally exhibited comparable fatigue resistance at room temperature, considering the variations in the strain rates during the tests (e.g., 0.006 s^{-1} of CLAM, 0.002±0.0006 s^{-1} of Eurofer97, and 0.01±0.003 s^{-1} of F82H) and variations in the tested sample sizes, from 2.7-mm-diameter Eurofer97 to 8-mm-diameter CLAM in the gauge section. However, CLAM seems to possess somewhat superior fatigue resistance compared with F82H at 550°C in air; this may be attributable to the higher tantalum content in CLAM, which favors smaller prior-austenite grains [22]. It is hard to determine the contribution of the Cr content (i.e., ~0.8% higher Cr in CLAM than in F82H) to the fatigue resistance because CLAM used noticeably larger test samples with a gauge diameter ~2.6 times that of F82H. The fatigue tests of Eurofer97 in vacuum at 550°C may have benefited the fatigue resistance, making it comparable to the resistance at room temperature.

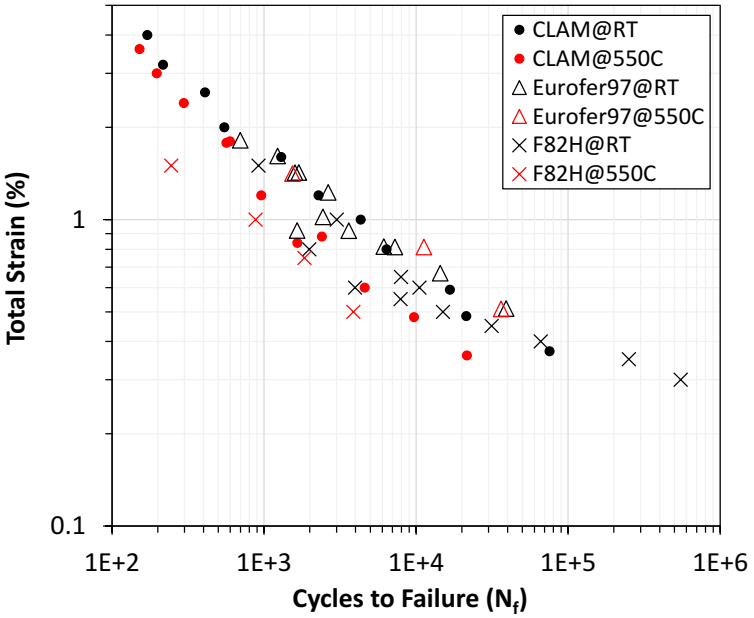

Fig. 3. Total strain and number of cycles to failure of CLAM, Eurofer97, and F82H tested at room temperature and 550°C.

3. Development of next-generation RAFM steels

To improve the performance of current RAFM steels, thermomechanical treatments (TMTs), including nonstandard heat treatments, and alloy chemistry refinement or modification have been the two primary routes.

3.1 TMTs and nonstandard heat treatments

Following a successful demonstration of improved strength in FM steels resulting from appropriate TMTs [44,45,46], similar TMTs were explored on RAFM steels; they achieved some promising improvements in strength, attributable to the refined subgrains and precipitates [10,11]. The effects of nonstandard heat treatments—such as normalization at 980, 1050, and 1150°C for 0.5 h, coupled with tempering at 700 and 760°C for 1.5 h—on the mechanical

properties of Eurofer97 were investigated recently. Figure 4 summarizes the resulting Charpy impact toughness (DBTT and USE) and tensile properties (TS, YS, TE, and uniform elongation [UE]) at 650°C, showing the dependence of USE, UE, TE, YS, and TS on DBTT. Miniature Charpy V-notch impact specimens (KLST type with a 3×3 mm^2 area under the V-notch) and tensile specimens (3 mm diameter by 15 mm length gauge) were used in the tests. The higher normalization temperature impaired the Charpy impact toughness by decreasing USE and increasing DBTT. However, it resulted in increased YS and TS with compromised UE and TE, which were attributed to the enlarged prior-austenite grain size. The reduction in Charpy impact toughness and increase in YS and TS became greater at the lower tempering temperature, which suggests that the highly supersaturated microstructure quenched from the higher normalization temperatures could not be appropriately relieved by the partial precipitation of carbides at the lower tempering temperature. The lower normalization temperature of 980°C generated a lower level of supersaturation that can be appropriately relieved at the lower tempering temperature of 700°C. Despite producing the highest impact toughness, the over-tempered condition of 980°C + 760°C resulted in not only the lowest strength but also a higher tendency toward a larger radiation-induced DBTT shift [47]. The study indicates that normalization and tempering temperatures of 1150°C + 760°C or 980°C + 700°C can be employed for Eurofer97 to develop greater strength and maintain decent impact toughness, compared with the generally employed heat treatments of ~1050°C + ~760°C. However, tempering at lower temperatures (e.g., 700°C) may be incompatible with the generally accepted practice of post-welding heat treatment; this possibility requires close examination and further development. Additionally, nonstandard heat treatments are not expected to noticeably alleviate or postpone thermal aging-induced property degradation, as discussed in Section 2.1.

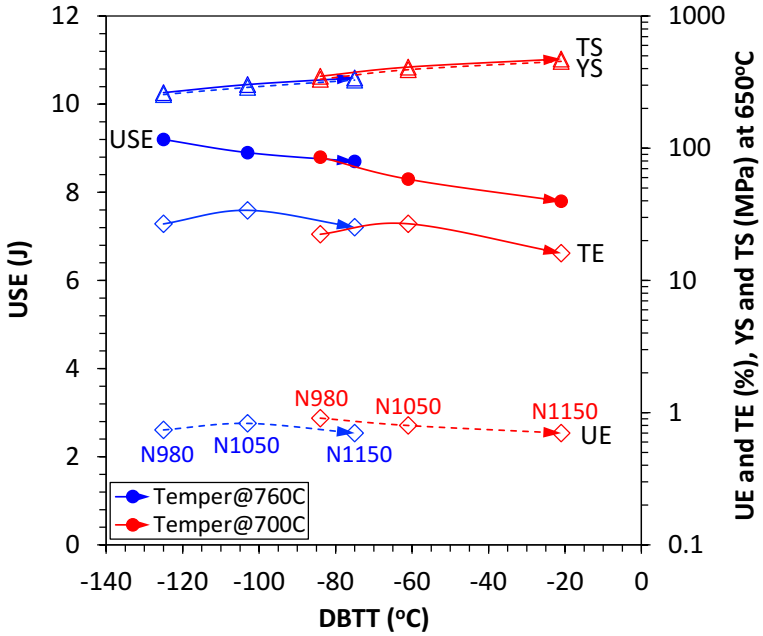

Fig. 4. Effects of nonstandard heat treatments—normalization at 980 (N980), 1050 (N1050), and 1150°C (N1150) and tempering at 700 and 760°C—on Charpy impact toughness (i.e., USE and DBTT, solid circles) and on tensile properties (i.e., YS and TS, open triangles; UE and TE, open diamonds) at 650°C.

3.2 Alloy chemistry refinement and modification

Alloy chemistry refinement has been explored for RAFM steels, leading to the evolution of Eurofer97-1 to Eurofer97-2 and the evolution of F82H-IEA to F82H-mod and F82H-BA. More dramatic alloy chemistry adjustments of RAFM steels have also been pursued. For instance, the addition of trace amounts of zirconium (<0.01 wt %) demonstrated some improvements in both impact and creep resistance, despite a negligible influence on yield strength [48]. Recently, ORNL has developed CNAs, which adjust the alloy chemistry by adding N or Ti and modifying relevant elements to balance austenite stabilizers such as C, N, and Mn with ferrite stabilizers such as Cr, W, Ta, V, Si, and Ti. The initial chemistry of CNAs is targeted in the range of 8.3–9.0 Cr, 1.0–1.5 W, <1.0 Mn, 0.1–0.3 V, 0.05–0.15 Ta, <0.2 Ti, <0.2 Si, 0.08–0.15 C, and <0.06 N, with iron as the balance in wt % [49]. Computational alloy thermodynamics, together with precipitate coarsening kinetics, was employed to help determine the range of the elements to favor a high density of ultrafine stable nanoprecipitates for superior high-temperature performance.

Two groups of CNAs were explored, including nitride-strengthened CNA1 (9Cr–1.1WVTaN), e.g., heat 1539 [10,11], and carbide-strengthened CNA2 and CNA3 (8.6Cr–1.3WVTaTi). Increased amounts of nitrogen in CNA1 and the addition of titanium in CNA2 and CNA3 significantly favor the formation of an MX phase. The increased amounts of nitrogen (<0.06) or added titanium (<0.2) comply with the reduced-activation concentration requirements [3], although the higher nitrogen content compromises low activation compared with the current RAFM steels. Figure 5 shows an example of the calculated temperature-dependent mole fraction of phases in CNA2 compared with that in Eurofer97. The MX phase in Eurofer97 is primarily composed of (V,Ta)N (i.e., MN), together with a trace amount of TaC (i.e., MC). The (V,Ta)N undergoes phase transformation into a coarse Z phase, e.g., Cr(V,Ta)N, at temperatures below ~800°C. In contrast, titanium is added in CNA2 and nitrogen is eliminated, preferentially yielding a large amount of (Ti,Ta)C (i.e., MC) and leading to a reduction in $M_{23}C_6$ because the carbon is consumed. Additionally, the absence of MN prevents Z phase formation in CNA2. The equilibrium calculation results indicate that thermal aging of current RAFM steels, as well as CNA1, at service-relevant temperatures (e.g., <~650°C) will result in increasing amounts of Laves, $M_{23}C_6$, and Z phases (compensated by reducing MN) compared with the initial tempered condition at ~750°C. The three increased phases are coarse particles, which would aggravate aging-induced property degradation, as discussed in Section 2.1. The absence of a Z phase in the carbide-strengthened steels CNA2 and CNA3 is expected to alleviate aging-induced property degradation. Furthermore, such degradations are expected to be mitigated by the increased number of MX nanoprecipitates, which help pin subgrain boundaries to reduce the recovery of subgrains and thus retard grain growth. These expectations will be verified by aging of the CNAs samples.

Transmission electron microscopy (TEM) was employed to characterize the microstructures of CNAs in a normalized and tempered condition, which were fabricated using the same steelmaking methods used for current RAFM steels. A high concentration of MC nanoprecipitates (~3–20 nm in diameter and of an order close to 10^{23} m^{-3} in the dark field image, Fig. 5a) and free dislocations (~4×10^{14} m^{-2} in the weak beam dark field image, Fig. 5b) were

observed in CNA2. The TEM images for CNA2 were compared with energy-dispersive x-ray spectroscopy (EDS) maps of V and Ta within an 18×18 μm^2 sampling area of Eurofer97 (Figs. 5c–d [50]), which show (V,Ta)N nanoprecipitates of ~10–50 nm on the order of 10^{20} m^{-3}. The results show that CNA2 possesses refined MX nanoprecipitates with a two orders-of-magnitude increase in number density. Electron probe microanalysis of the V/Ta distribution within a 30×22 μm^2 sampling area of F82H–BA07 [51] and –BA12 [52] showed an MX distribution similar to that in Eurofer97. The larger amount of MC in CNA2, compared with Eurofer97 and F82H, is approximately consistent with the thermodynamic phase fraction calculations of the alloys. The higher density of smaller MX nanoprecipitates in the CNAs yielded noticeable increases in yield and tensile strength with compromised ductility [49].

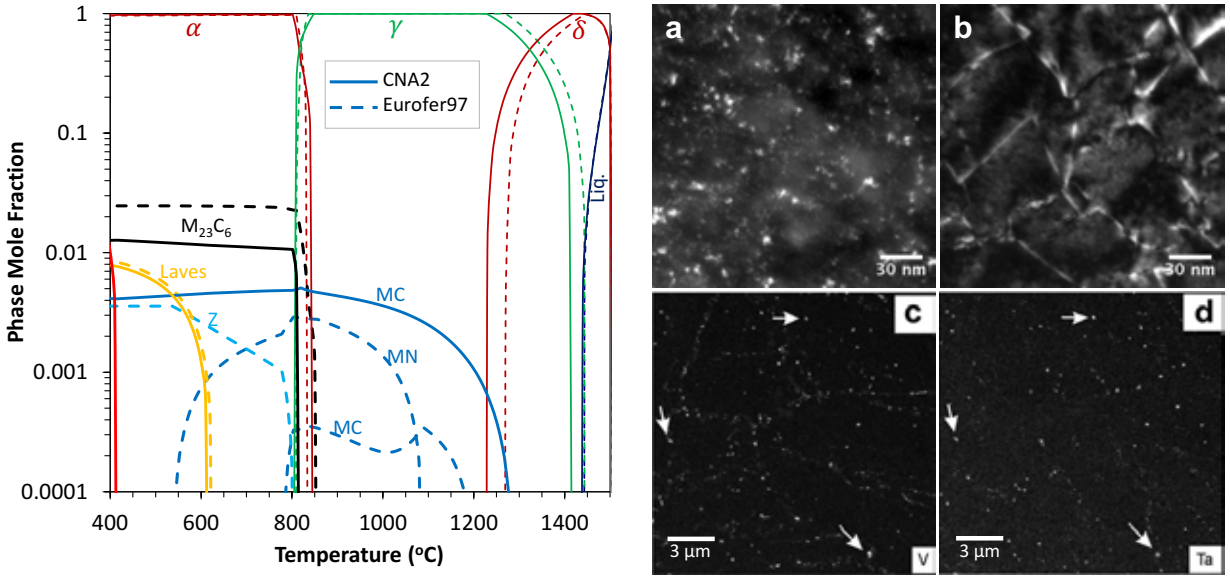

Fig. 5. Calculated temperature-dependent mole fraction of precipitates in CNA2 and Eurofer97, together with the microstructures of (a) MX nanoprecipitates and (b) dislocations in CNA2 compared with (c-d) the EDS-maps of V and Ta in Eurofer97 [50].

The impact toughness of CNAs was assessed using half-size Charpy V-notch specimens. Figure 6 shows the results for CNAs compared with literature data for Grade 91 [53]; all of the specimens were tested in the T–L specimen orientation. The data are fitted by a hyperbolic tangent function $E = a + b \tanh[(T - T_0)/c]$, where T is test temperature and a, b, c and T_0 are regression coefficients. The T_0 gives the mathematical DBTT, corresponding to the mean value of USE and lower-shelf energy (LSE); i.e., 1/2USE assuming LSE = 0 in Fig. 6. The nitride-strengthened CNA1 exhibited impact toughness comparable to that of Grade 91. In contrast, carbide-strengthened CNA2 and CNA3 showed significant increases in USE, up to ~70 J; they also had comparable or lower DBTT, although the same normalization and tempering conditions were applied to the CNAs. The enhanced impact toughness of the carbide-strengthened CNAs is attributable to the refined grain structure and increased manganese content (e.g., to ~0.8% in CNA3). The USE of the CNAs was dramatically higher than that of 9–20Cr oxide-dispersion-strengthened (ODS) ferritic steels (e.g., the average USE of the ODS steels is schematically shown with a dashed line in Fig. 6 [49]).

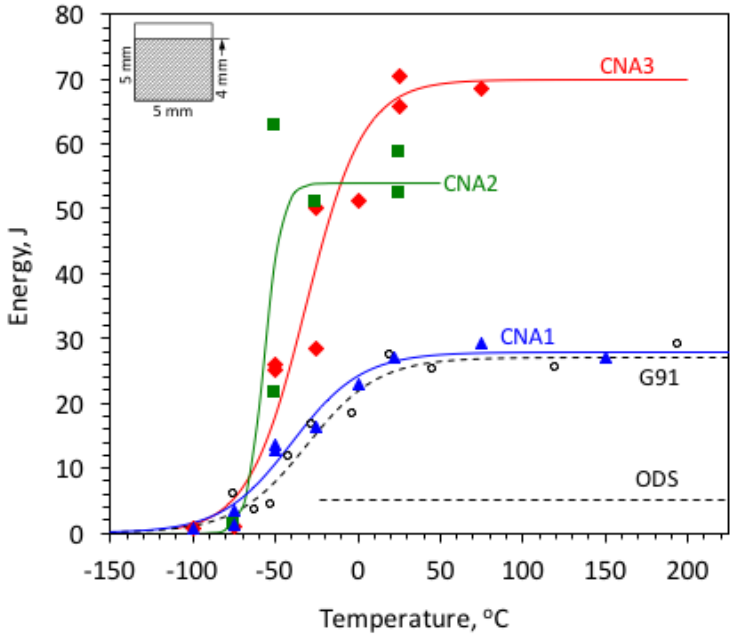

Fig. 6. Charpy V-notch impact toughness of CNAs compared with Grade 91 [53] and oxide-dispersion-strengthened steels (ODS). The cross-section of the V-notch specimens is shown in the inset.

3.3 Creep resistance

Figure 7 shows the creep rupture life of Eurofer97 (solid circles) [54] and F82H-IEA (crosses) [55,56] at 50–300 MPa and 500–650°C. It indicates that F82H has comparable or slightly superior creep resistance. The F82H data at each temperature are fitted with a solid line and with a dashed line extrapolating to 40 years. The specimens were tested in vacuum, except for two of the F82H specimens tested at 650°C in air; the latter showed significantly shorter creep rupture lives (not included in the fitting). The specimens were extracted from different forms of products: 7.5 to 25-mm-thick plates for F82H, and 14-mm-thick plates and 100-mm-diameter rods for Eurofer97. The product form did not appear to have a significant effect on the creep resistance. The data show decreased creep resistance at higher temperatures, with accelerated degradation when the time to rupture is beyond ~10,000 h above 550°C. Following the general creep resistance phenomena in 9–12Cr FM steels, the accelerated degradation in creep resistance is believed to be attributable to the stress-accelerated formation and coarsening of the Laves, Z, and $M_{23}C_6$ phases in the alloys, which could not hamper the recovery of the subgrains. Long-term low-stress creep tests are needed to verify the extrapolated dashed lines predicting the accelerated degradation. The limited high-temperature creep resistance of the current RAFM steels is a critical life-limiting factor for their DEMO applications.

Preliminary creep rupture data for CNA2 (solid triangles) tested at 110 MPa and 650°C in air are included in Fig. 7, which shows an ~20 MPa increase in creep stress and an increase of about one order of magnitude in creep life compared with Eurofer97 and F82H. The data for CNA2 were generated from type SS-3 miniature specimens extracted from an 8-mm-thick plate with a gauge cross-section of 1.52×0.76 mm^2. They were significantly smaller than the standard

specimens used for F82H and Eurofer97, e.g., an 8-mm-diameter gauge cross-section of Eurofer97. The use of the miniature specimens at 650°C in air may have compromised the creep rupture lives of CNA2 somewhat. Creep tests of CNAs using larger specimens at multiple temperature and load conditions are in progress.

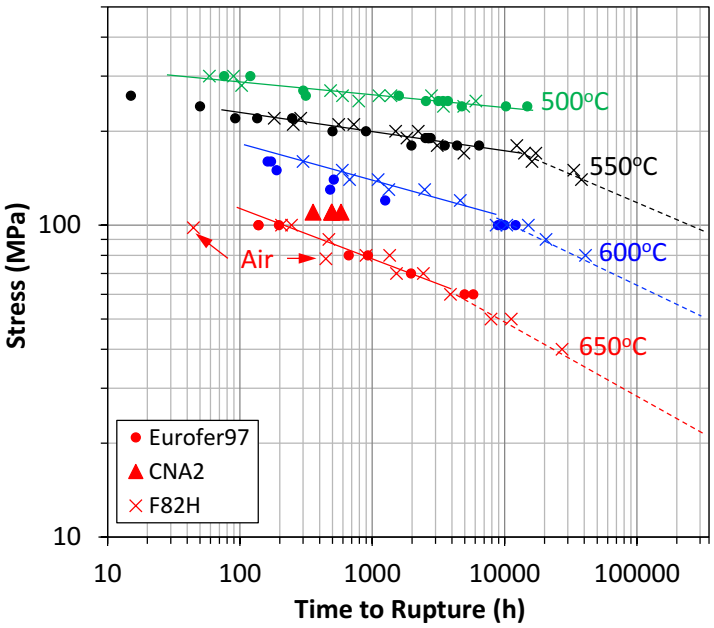

Fig. 7. Creep resistance of CNA2 compared with Eurofer97 [54] and F82H [55,56] with trend lines for F82H.

3.4 Radiation hardening

Many neutron irradiation experiments have been conducted on Eurofer97 and F82H. Post-irradiation tensile tests were usually performed at both room temperature and the irradiation temperatures to evaluate radiation hardening. Figure 8 shows the measured changes in YS and TE after irradiation at room temperature, compared with their values before irradiation (YS_0 and TE_0), as a function of irradiation dose for Eurofer97 (solid circles) and F82H (solid and open diamonds) irradiated at ~300–325°C. The Eurofer97 data include the results generated from the EB2, HFR, SUMO-02, SPICE, and BOR60 reactors [57,58,59]. The radiation hardening data for Eurofer97 in Fig. 8a are approximately fitted with a generally employed function $\Delta\sigma_{YS} = \Delta\sigma_0\sqrt{1-e^{(-\phi/\phi_0)}}$ with ϕ, ϕ_0, and $\Delta\sigma_0$ representing the irradiation dose, the fitting results of the irradiation dose and the maximum saturated increase in YS, respectively. The Eurofer97 hardening was still not saturated at the high dose of 70 dpa generated in the BOR60; this may be attributed to reactor differences in dpa rate, neutron spectrum, and so on. The F82H data include the results obtained from the Osiris and HFIR irradiations [59,60] and generally show lower radiation hardening than the Eurofer97 data. Compared with the F82H-IEA (solid diamonds), different versions of F82H-mod (open diamonds) exhibit comparable or lower radiation hardening. In contrast to the general observations of lower radiation hardening for the F82H-IEA heat, accompanied by smaller reductions in TE – TE_0 compared with Eurofer97, the F82H-mod variants exhibit lower radiation hardening but noticeably larger reductions in TE – TE_0 (Fig. 8b).

These results suggest poor radiation resistance of F82H-mod. Only one datum for CLAM (crosses) was generated using China's High Flux Engineering Test Reactor (HFETR) at 300°C. It shows noticeably lower hardening but approximately follows the trend of reduced TE – TE_0. A set of nitride-strengthened CNA1 tensile specimens were irradiated in the HFIR at 300°C for up to 5 dpa. The two low-dpa data points for CNA1 (solid squares) approximately follow the trend of the F82H-IEA and Eurofer97 data. The small radiation hardening (<80 MPa) did not impair the ductility of CNA1 at such low doses. More post-irradiation examination and HFIR neutron irradiation experiments on CNAs are in progress or are planned to provide a more complete picture of radiation resistance.

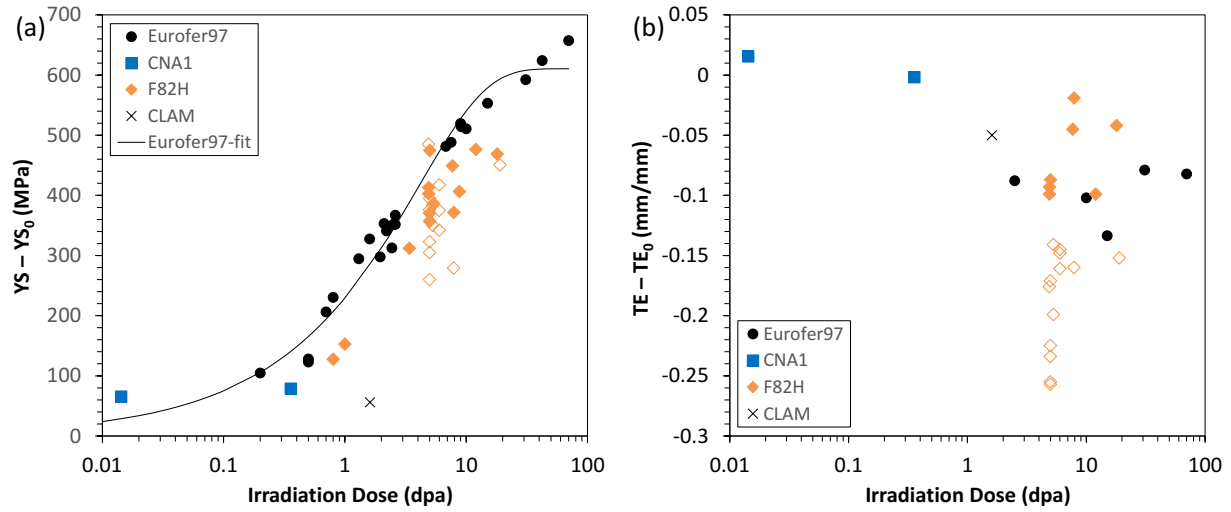

Fig. 8. Dose-dependent radiation-induced changes in (a) yield strength and (b) total elongation of Eurofer97 [57,58,59], F82H [59,60], CLAM, and CNA1 steel samples irradiated at ~300–325°C. All data are room-temperature tests.

Because of the low rates of helium production in the fission reactor experiments, surrogate irradiation experiments were pursued to explore the effects of helium level in a fusion spectrum on microstructural and mechanical properties of CNAs and RAFM steels. The experiments included ion irradiation with a dual beam (He + Fe) [61]; fission reactor irradiation of steels either coated with a thin NiAl layer [62] or doped with isotopes of ^{10}B, ^{58}Ni, or ^{54}Fe; and spallation neutron irradiation, although it produces more helium than a fusion spectrum. Dual-beam ion irradiation of F82H-mod3 at 500°C to up to 60 dpa and 2100 atomic parts per million (appm) helium generated a moderate density (~3×10^{22} m^{-3}) of nonuniformly distributed cavities with bimodal sizes ranging from ~1 nm helium bubbles up to ~20 nm faceted voids, corresponding to ~0.44% swelling [61]. Correlations between the precipitates and the distribution of the bubbles and voids were not observed. An in situ helium-implanter experiment on F82H-mod3 coated with a NiAl layer, conducted at HFIR at 500°C to ~9 dpa and 190 or 380 appm helium, suggested a high density (~5×10^{22} m^{-3}) of ~2 nm helium bubbles, together with significantly fewer ~10 nm faceted voids [62]. The bubbles preferentially formed on boundaries and dislocations, a condition that may result in premature embrittlement. Recent dual-beam ion irradiation experiments, at 650°C to ~50 dpa with an ~15 appm helium/dpa ratio, indicated a moderate capability to manage helium by trapping it at ultrafine (Ti,Ta)C precipitates in the matrix of CNA3 [63]. This suggests a potential alleviation of helium effects on swelling and

embrittlement. CLAM steels recently completed high-energy spallation neutron irradiation at 56–470°C up to 21 dpa at the Swiss spallation neutron source (SINQ). F82H and US 9Cr-2WVTa doped with ^{10}B or ^{58}Ni isotopes recently completed neutron irradiation at 300–650°C to >80 dpa at HFIR. Purification of the ^{54}Fe isotope has been completed recently, and it will be alloyed with CNAs and Eurofer97 for neutron irradiation experiments at HFIR. The results from these recently completed and ongoing irradiation experiments will provide a solid foundation for the development and deployment of RAFM steels and CNAs in DEMO and later fusion reactors.

4. Summary

The research and development history and current status of 9Cr RAFM steels were briefly reviewed, from small lab heats to large industrial-scale heats of steel larger than 20 tons. A comprehensive set of properties of RAFM steels were investigated, including the recent stringent activity for code qualification of Eurofer97 to RCC-MRx edition 2015. A few aspects of current RAFM steels were discussed. Long-term thermal aging resulted in reductions in strength and ductility and degradation of Charpy impact toughness at aging temperatures above 500°C for F82H, Eurofer97, and CLAM. An increase in plate thickness from ~15 to 100 mm resulted in some reductions in the Charpy impact energy but little influence on the tensile properties of F82H and CLAM. The recent addition of fracture toughness data for Eurofer97-1 in the transition regime increased the scatter in the database, which yielded a modification of the master curve but retained the same T_0 of –90°C, up to 29°C higher than the T_0 of F82H. Comparable fatigue resistance was observed for F82H, Eurofer97, and CLAM at room temperature. However, CLAM seems to possess somewhat superior fatigue resistance in air at 550°C compared with F82H.

TMTs, including nonstandard heat treatments, and alloy chemistry refinement or modification have been employed in the development of next-generation RAFM steels for superior performance. Lower normalization and tempering temperatures (e.g., 980 and 700°C) were found to produce similar balanced strength and Charpy impact toughness compared with Eurofer97 normalized and tempered at higher temperatures (e.g., 1150 and 760°C). CNAs recently developed at ORNL exhibited significantly increased amounts of ultrafine MX nanoprecipitates, leading to promising improvements in strength, creep resistance, and impact toughness compared with current RAFM steels. Preliminary neutron irradiation results for one of the CNAs showed radiation hardening comparable to that shown in the large database for Eurofer97 and F82H. Ongoing research and development activities on RAFM steels and CNAs will provide a solid foundation for their deployment in DEMO and later fusion reactors.

Acknowledgment

This research was supported by the U.S. Department of Energy, Office of Science, Fusion Energy Sciences. This manuscript was authored by UT-Battelle, LLC, under contract number DE-AC05-00OR22725 with the U.S. Department of Energy. Part of this work was supported by the EUROfusion Consortium through the Euratom research and training programme, "Broader Approach Agreement" between the Government of Japan and the Euratom, and the National

Basic Research Program of China. The authors thank F.W. Wiffen and S.J. Zinkle for useful discussions.

References

[1] A. Kohyama, A. Hishinuma, D.S. Gelles, R.L. Klueh, W. Dietz, K. Ehrlich, J. Nucl. Mater. 233–237 (1996) 138–147.
[2] K.J. Harrelson, S.H. Rou, R.C. Wilcox, J. Nucl. Mater. 141-143 (1986) 508–512.
[3] R.L. Klueh, E.T. Cheng, M.L. Grossbeck, E.E. Bloom, J. Nucl. Mater. 280 (2000) 353–359.
[4] H. Tanigawa, Y. Someya, H. Sakasegawa, T. Hirose, K. Ochiai, Radiological assessment of the limits and potential of reduced activation ferritic/martensitic steels, Fus. Eng. Des. 89 (2014) 1573–1578.
[5] Q. Huang, J. Li, Y. Chen, Study of irradiation effects in China low activation martensitic steel CLAM, J. Nucl. Mater. 329–333 (2004) 268–272.
[6] R.L. Klueh, Heat treatment behavior and tensile properties of Cr–W steels, Metall. Trans. A 20 (1989) 463–470.
[7] R.L. Klueh, P.J. Maziasz, The microstructure of chromium-tungsten steels, Metall. Trans. A 20 (1989) 373–382.
[8] R.L. Klueh, W.R. Corwin, Impact behavior of Cr–W steels, J. Mater. Eng. 11 (1989) 169–175.
[9] R.L.Klueh, Reduced activation status: future development for improved creep strength, J. Nucl. Mater. 378 (2008) 159–166.
[10] L. Tan, D.T. Hoelzer, J.T. Busby, M.A. Sokolov, R.L. Klueh, Microstructure control for high strength 9Cr ferritic-martensitic steels, J. Nucl. Mater. 422 (2012) 45–50.
[11] L. Tan, Y. Yang, J.T. Busby, Effects of alloying elements and thermomechanical treatment on 9Cr reduced activation ferritic-martensitic (RAFM) steels, J. Nucl. Mater. 442 (2013) S13–S17.
[12] M. Tamura, H. Hayakawa, M. Tanimura, A. Hishinuma, T. Kondo, J. Nucl. Mater. 141–143 (1986) 1067–1073.
[13] K. Asakura, T. Fujita, Elevated temperature strength and toughness of ferritic steels, J. Japan Atomic Energy Soc. 28 (1986) 222–231.
[14] R. Lindau, A. Möslang, M. Rieth, M. Klimiankou, E. Materna-Morris, A. Alamo, A.-A.F. Tavassoli, C. Caryon, A.-M. Lancha, P. Fernandez, N. Baluc, R. Schäublin, E. Diegele, G. Filacchioni, J.W. Rensman, B. van der Schaaf, E. Lucon, W. Dietz, Fusion Eng. Des. 75–79 (2005) 989–996.
[15] Q. Huang, N. Baluc, Y. Dai, S. Jitsukawa, A. Kimura, J. Konys, R.J. Kurtz, R. Lindau, T. Muroga, G.R. Odette, B. Raj, R.E. Stoller, L. Tan, H. Tanigawa, A.-A.F. Tavassoli, T. Yamamoto, F. Wan, Y. Wu, Recent progress of R&D activities on reduced activation ferritic/martensitic steels, J. Nucl. Mater. 442 (2013) S2–S8.
[16] Q. Huang, FDS Team, Development status of CLAM steel for fusion application, J. Nucl. Mater. 455 (2014) 649–654.
[17] S. Banerjee, Overview of Indian activities on fusion reactor materials, J. Nucl. Mater. 455 (2014) 217–224.

[18] Y.B. Chun, S.H. Kang, S. Noh, T.K. Kim, D.W. Lee, S. Cho, Y.H. Jeong, Effects of alloying elements and heat treatments on mechanical properties of Korean reduced-activation ferritic-martensitic steel, J. Nucl. Mater. 455 (2014) 212–216.
[19] NRIM Creep Data Sheet No. 43, National Research Institute for Metals, Japan, 1996.
[20] H. Tanigawa, K. Shiba, H. Sakasegawa, T Hirose, S. Jitsukawa, Technical issues related to the development of reduced-activation ferritic/martensitic steels as structural materials for fusion blanket system, Fus. Eng. Des. 86 (2011) 2549–2552.
[21] M. Rieth, J. Rey, Specific welds for test blanket modules, J. Nucl. Mater. 386–388 (2009) 471–474.
[22] A.-A.F. Tavassoli, E. Diegele, R. Lindau, N. Luzginova, H. Tanigawa, Current status and recent research achievements in ferritic/martensitic steels, J. Nucl. Mater. 455 (2014) 269–276.
[23] H. Tanigawa, K. Shiba, A. Moeslang, R.E. Stoller, R. Lindau, M.A. Sokolov, G.R. Odette, R.J. Kurtz, S. Jitsukawa, Status and key issues of reduced activation ferritic/martensitic steels as the structural material for a DEMO blanket, J. Nucl. Mater. 417 (2011) 9–15.
[24] P. Aubert, F. Tavassoli, M. Rieth, E. Diegele, Y. Poitevin, Review of candidate welding processes of RAFM steels for ITER test blanket modules and DEMO, J. Nucl. Mater. 417 (2011) 43–50.
[25] H. Tanigawa, T. Hirose, K. Shiba, B.R. Kasada, E. Wakaia, H. Serizawa, Y. Kawahito, S. Jitsukawa, A. Kimura, Y. Kohno, A. Kohyama, S. Katayama, H. Mori, K. Nishimoto, R.L. Klueh, M.A. Sokolov, R.E. Stoller, S.J. Zinkle, Technical issues of reduced activation ferritic/martensitic steels for fabrication of ITER test blanket modules, Fus. Eng. Des. 83 (2008) 1471–1476.
[26] S. Smolentsev, N.B. Morley, M.A. Abdou, S. Malang, Dual-coolant lead-lithium (DCLL) blanket status and R&D needs, Fus. Eng. Des. 100 (2015) 44–54.
[27] A. Kimura, R. Kasada, A. Kohyama, S. Konishi, M. Enoeda, M. Akiba, S. Jitsukawa, S. Ukai, I. Terai, A. Sagara, Ferritic steel-blanket systems integration R&D – compatibility assessment, Fus. Eng. Des. 81 (2006) 909–916.
[28] V. Shankar, K. Mariappan, R. Sandhya, K. Laha, T. Jayakumar, E.R. Kumar, Effect of W and Ta on creep-fatigue interaction behavior of reduced activation ferritic-martensitic (RAFM) steels, Fus. Eng. Des. 100 (2015) 314–320.
[29] T. Hirose, M.A. Sokolov, M. Ando, H. Tanigawa, K. Shiba, R.E. Stoller, G.R. Odette, Irradiation response in weldment and HIP joint of reduced activation ferritic/martensitic steel, F82H, J. Nucl. Mater. 442 (2013) S557–S561.
[30] E. Materna-Morris, A. Moslang, H.C. Schneider, Tensile and low cycle fatigue properties of Eurofer97-steel after 16.3 dpa neutron irradiation at 523, 623, and 723 K, J. Nucl. Mater. 442 (2013) S62–S66.
[31] A. Alamo, J.L. Bertin, V.K. Shamardin, P. Wident, Mechanical properties of 9Cr martensitic steels and ODS-FeCr alloys after neutron irradiation at 325 degrees C up to 42 dpa, J. Nucl. Mater. 367 (2007) 54–59.
[32] K. Shiba, H. Tanigawa, T. Hirose, H. Sakasegawa, S. Jitsukawa, Long-term properties of reduced activation ferritic/martensitic steels for fusion reactor blanket system, Fus. Eng. Des. 86 (2011) 2895–2899.
[33] M. Tamura, K. Shinozuka, H. Esaka, S. Sugimoto, K. Ishizawa, K. Masamura, Mechanical properties of 8Cr–2WVTa steel aged for 30,000 h, J. Nucl. Mater. 283–287 (2000) 667–671.

[34] L. Stratil, H. Hadraba, J. Bursik, I. Dlouhy, Comparison of microstructural properties and Charpy impact behavior between different plates of the Eurofer97 steel and effect of isothermal ageing, J. Nucl. Mater. 416 (2011) 311–317.
[35] H. Sakasegawa, H. Tanigawa, Mechanical properties of F82H plates with different thicknesses, Fus. Eng. Des. (2015) in press.
[36] G.R. Odette, T. Yamamoto, H. Kishimoto, M. Sokolov, P. Spätig, W.J. Yang, J.-W. Rensman, G.E. Lucas, A master curve analysis of F82H using statistical and constraint loss size adjustments of small specimen data, J. Nucl. Mater. 329–333 (2004) 1243–1247.
[37] B.J. Kim, R. Kasada, A. Kimura, E. Wakai, H. Tanigawa, Application of master curve method to the evaluation of fracture toughness of F82H steels, J. Nucl. Mater. 442 (2013) S38–S42.
[38] X. Hu, L. Huang, W. Wang, Z. Yang, W. Sha, W. Wang, W. Yan, Y. Shan, Low cycle fatigue properties of CLAM steel at room temperature, Fus. Eng. Des. 88 (2013) 3050–3059.
[39] X. Hu, L. Huang, W. Yan, W. Wang, W. sha, Y. Shan, K. Yang, Low cycle fatigue properties of CLAM steel at 823 K, Mater. Sci. Eng. A 613 (2014) 404–413.
[40] P. Marmy, T. Kruml, Low cycle fatigue of Eurofer 97, J. Nucl. Mater. 377 (2008) 52–58.
[41] J.F. Stubbins, D.S. Gelles, Fatigue performance and cyclic softening of F82H, a ferritic-martensitic steel, J. Nucl. Mater. 233–237 (1996) 331–335.
[42] A.-A.F. Tavassoli, J.-W. Rensman, M. Schirra, K. Shiba, Materials design data for reduced activation martensitic steel type F82H, Fus. Eng. Des. 62–62 (2002) 617–628.
[43] M.A. Meyers, K.K. Chawla, Mechanical Behavior of Materials, Cambridge University Press, New York, 2009, p.718.
[44] R.L. Klueh, N. Hashimoto, P.J. Maziasz, Development of new nano-particle-strengthened martensitic steels, Scripta Mater. 53 (2005) 275–280.
[45] S. Hollner, B. Founier, J. Le Pendu, T. Cozzika, I. Tournié, J.-C. Brachet, A. Pineau, High-temperature mechanical properties improvement on modified 9Cr–1Mo martensitic steel through thermomechanical treatments, J. Nucl. Mater. 405 (2010) 101–108.
[46] L. Tan, J.T. Busby, P.J. Maziasz, Y. Yamamoto, Effect of thermomechanical treatment on 9Cr ferritic-martensitic steels, J. Nucl. Mater. 441 (2013) 713–717.
[47] E. Gaganidze, H.-C. Schneider, B. Dafferner, J. Aktaa, Embrittlement behavior of neutron irradiated RAFM steels, J. Nucl. Mater. 367–370 (2007) 81–85.
[48] Y.B. Chun, S.H. Kang, S. Noh, T.K. Kim, D.W. Lee, S. Cho, Y.H. Jeong, Effects of alloying elements and heat treatments on mechanical properties of Korean reduced-activation ferritic-martensitic steel, J. Nucl. Mater. 455 (2014) 212–216.
[49] L. Tan, L.L. Snead, Y. Katoh, Development of new generation reduced activation ferritic-martensitic steels for advanced fusion reactors, submitted to J. Nucl. Mater. (2016).
[50] M. Klimenkov, R. Lindau, E. Matema-Morris, A. Möslang, TEM characterization of precipitates in Eurofer 97, Prog. Nucl. Energy 57 (2012) 8–13.
[51] H. Sakasegawa, H. Tanigawa, S. Kano, M. Enomoto, Precipitation behavior in F82H during heat treatments of blanket fabrication, Fus. Eng. Des. 86 (2011) 2541–2544.
[52] H. Sakasegawa, H. Tanigawa, S. Kano, H. Abe, Material properties of the F82H melted in an electric arc furnace, Fus. Eng. Des. 98–99 (2015) 2068–2071.
[53] W.R. Corwin, A.M. Hougland, Effect of specimen size and material condition on the Charpy impact properties of 9Cr-1Mo-V-Nb steel, in: W.R. Corwin, G.E. Lucas (Eds.), The

Use of Small-Scale Specimens for Testing Irradiated Material, ASTM STP 888, American Society for Testing and Materials, Philadelphia, 1986, pp. 325-338.
[54] M. Rieth, M. Schirra, A. Falkenstein, P. Graf, S. Heger, H. Kempe, R. Lindau, H. Zimmermann, Eurofer 97 tensile, Charpy, creep and structural tests, Forschungszentrum Karlsruhe in der Helmholtz-Gemeinschaft, Wissenschaftliche Berichte FZKA 6911, October 2003.
[55] A.-A.F. Tavassoli, J.-W. Rensman, M. Schirra, K. Shiba, Materials design data for reduced activation martensitic steel type F82H, Fusion Engineering and Design 61-62 (2002) 617-628.
[56] M. Tamura, M.M. Nowell, K. Shinozuka, H. Esaka, Creep behavior of double tempered 8%Cr-2%WVTa martensitic steel, Mater. Trans. 47 (2006) 1332-1340.
[57] E. Gaganidze, C. Petersen, Poste irradiation examination of RAFM steels after fast reactor irradiation up to 71 dpa and <340C (ARBOR 2), KIT Scientific Reports 7596, 2011.
[58] C. Petersen, Poste irradiation examination of RAF/M steels after fast reactor irradiation up to 33 dpa and <340C (ARBOR 1), Forschungszentrum Karlsruhe, FZKA7517, Novermber 2010.
[59] E. Lucon, P. Benoit, P. Jacquet, E. Diegele, R. Lasser, A. Alamo, R. Coppola, F. Gillemot, P. Jung, A. Lind, S. Messoloras, P. Novosad, R. Lindau, D. Preininger, M. Klimiankou, C. Pertersen, M. Rieth, E. Materna-Morris, H.-C. Schneider, J.-W. Rensman, B. van der Schaaf, B.K. Singh, P. Spaetig, The Europen effort towards the development of a demo structural material: irraidation behaviour of the European reference RAFM steel Eurofer, Fus. Eng. Des. 81 (2006) 917–923.
[60] T. Hirose, N. Okubo, H. Tanigawa, M. Ando, M.A. Sokolov, R.E. Stoller, G.R. Odette, Irradiation hardening in F82H irradiated at 573 K in the HFIR, J. Nucl. Mater. 417 (2011) 108–111.
[61] T. Yamamoto, Y. Wu, G.R. Odette, K. Yabuuchi, S. Kondo, A. Kimura, A dual ion irradiation study of helium-dpa interactions on cavity evolution in tempered martensitic steels and nanostructured ferritic alloys, J. Nucl. Mater. 449 (2014) 190–199.
[62] T. Yamamoto, G.R. Odette, P. Miao, D.J. Edwards, R.J. Kurtz, Helium effects on microstructural evolution in tempered martensitic steels: in situ helium implanter studies in HFIR, J. Nucl. Mater. 386–388 (2009) 338–341.
[63] C.M. Parish, K.A. Unocic, L. Tan, S.J. Zinkle, S. Kondo, L.L. Snead, D.T. Hoelzer, Y. Katoh, Sequestration of cavities at nanoparticle-matrix interfaces in helium + heavy ion irradiated nanostructured ferritic alloys, submitted to J. Nucl. Mater. (2015).